

# T-SCEND: Test-time Scalable MCTS-enhanced Diffusion Model

Tao Zhang<sup>\*1</sup> Jia-Shu Pan<sup>\*1</sup> Ruiqi Feng<sup>1</sup> Tailin Wu<sup>\*†1</sup>

## Abstract

We introduce *Test-time Scalable MCTS-enhanced Diffusion Model* (T-SCEND), a novel framework that significantly improves diffusion model’s reasoning capabilities with better energy-based training and scaling up test-time computation. We first show that naïvely scaling up inference budget for diffusion models yields marginal gain. To address this, the training of T-SCEND consists of a novel linear-regression negative contrastive learning objective to improve the *performance-energy consistency* of the energy landscape, and a KL regularization to reduce *adversarial sampling*. During inference, T-SCEND integrates the denoising process with a novel hybrid Monte Carlo Tree Search (hMCTS), which sequentially performs best-of-N random search and MCTS as denoising proceeds. On challenging reasoning tasks of Maze and Sudoku, we demonstrate the effectiveness of T-SCEND’s training objective and scalable inference method. In particular, trained with Maze sizes of up to  $6 \times 6$ , our T-SCEND solves 88% of Maze problems with much larger sizes of  $15 \times 15$ , while standard diffusion completely fails. Code to reproduce the experiments can be found at [https://github.com/AI4Science-WestlakeU/t\\_scend](https://github.com/AI4Science-WestlakeU/t_scend).

## 1. Introduction

In recent years, diffusion generative models (Sohl-Dickstein et al., 2015; Ho et al., 2020; Song et al., 2021) have demonstrated remarkable performance across a wide range of applications, including image (Rombach et al., 2022) and video generation (Brooks et al., 2024), robotic control (Janner et al., 2022), and reasoning (Du et al., 2024). By learning how to denoise from noisy, corrupted samples to clean data samples, diffusion models can generate high-quality, high-dimensional samples approximating the data distribution.

<sup>\*</sup>Equal contribution <sup>†</sup>Corresponding author <sup>1</sup>Department of Artificial Intelligence, Westlake University. Correspondence to: Tailin Wu <wutailin@westlake.edu.cn>.

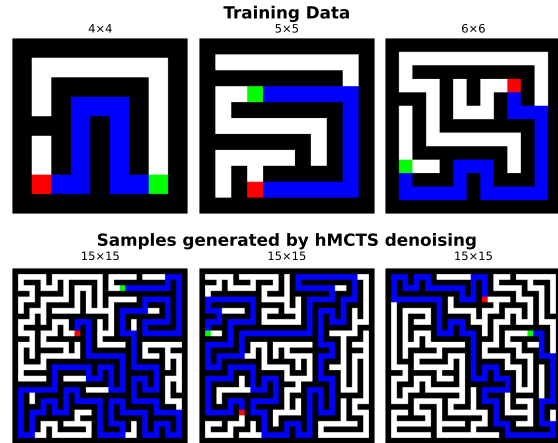


Figure 1. Visualizations of Maze training data and solutions generated by hMCTS denoising of our T-SCEND framework.

Nevertheless, as the application scenarios for diffusion models become more complex, they often encounter situations where the problem sizes are much larger than those in training or their conditional input is out-of-distribution (OOD). When dealing with larger problem sizes, the computational resources required may increase exponentially, and the existing models may struggle to maintain high-quality performance. In OOD scenarios, the diffusion models need to generalize to conditions that have characteristics different from what they have been trained on. Thus, the pressing question is how to further enhance the performance of diffusion models under such challenging circumstances.

Interestingly, test-time scaling has demonstrated its effectiveness in other generative AI methods such as large language models (Wei et al., 2022; Yao et al., 2024). It remains an interesting question whether test-time<sup>1</sup> scaling can also benefit diffusion models and address the challenges above.

However, naïve test-time scaling up for diffusion models by increasing denoising steps typically yields marginal gain after a certain number of function evaluations (NFEs), which was observed in prior works (Karras et al., 2022; Song et al., 2021). Another scaling-up dimension is the number of samples, while in our pivot study, best-of-N sampling with

<sup>1</sup>In this paper, we use “test-time” and “inference” interchangeably.

diffusion model still doesn't scale up significantly. Through analysis, we identify that the reason comes from both training and inference. For *training*, the model's performance is fundamentally upper-limited by the learned energy landscape<sup>2</sup>. For example, if the energy landscape has many local minima or has the wrong global minima, simply scaling up the inference budget will likely not result in improved performance. We identify that the insufficient *performance-energy consistency* and *adversarial sampling*<sup>3</sup> as two key reasons limiting the performance. These factors make the sampling easier to be stuck at sub-optimal solutions and hard to go out. For *inference*, simple search methods such as random search may not be efficient enough to navigate the vast space when generating high-dimensional samples.

In this work, we introduce *Test-time Scalable MCTS-enhanced Diffusion Model* (T-SCEND), a novel framework that significantly improves diffusion model's reasoning capability. T-SCEND consists of innovations in both training objectives and inference scaling. On the training side, T-SCEND incorporates a novel Linear-Regression Negative Contrastive Learning (LRNCL) objective to improve the *performance-energy consistency* of the energy landscape, and a KL regularization to address adversarial sampling. Specifically, for the LRNCL objective, it randomly samples two negative samples from a positive sample and performs a linear regression for these three samples on their energy vs. L2 distance to the positive sample. The LRNCL objective encourages that the samples' energy is linear w.r.t. their L2 distance to the positive sample, and the slope is positive, thus making the energy landscape reflective of their distance to the ground-truth, improving *performance-energy consistency*. For the KL regularization, it differentiates through the denoising process, making the energy landscape easier to sample and reducing *adversarial sampling*.

On the inference side, we integrate the denoising process with a novel hybrid Monte Carlo Tree Search (hMCTS). It sequentially performs best-of-N random search and MCTS as the denoising proceeds. The first few steps of best-of-N random search use  $L$  independent samples that denoise from the prior (Gaussian) distribution until reaching a predefined denoising step. The best sample is chosen from the  $L$  samples. Then MCTS denoising follows and completes the denoising process. The random search in the initial denoising steps allows the model to reach cleaner samples with a reasonable signal-to-noise ratio, while the later MCTS denoising allows better navigation in the search space. Taken

<sup>2</sup>We can regard diffusion model's denoising network  $\epsilon_\theta(\mathbf{x}_t, t)$  as approximating the gradient of an implicit energy function  $\nabla_{\mathbf{x}_t} E_\theta(\mathbf{x}_t, t)$ . The energy function connects to the probability distribution via  $p(\mathbf{x}) \propto e^{-E_\theta(\mathbf{x}, t=0)}$ . Thus, the lower the energy, the higher the probability. See Du et al. (2023) for more details.

<sup>3</sup>Detailed description for *performance-energy consistency* and *adversarial sampling* can be found in Appendix A.

together, the hybrid MCTS denoising allows the model to significantly improve inference performance by scaling up the inference computational budget.

We demonstrate the effectiveness of our T-SCEND's training objective and scalable inference method on challenging reasoning tasks of Maze and Sudoku. In Sudoku tasks, our T-SCEND solves 43% problems when conditioned on much less given digits (OOD condition), while the standard diffusion model only solves 30% problems. In Maze tasks, trained with Maze sizes of up to  $6 \times 6$ , our T-SCEND solves 88% of Maze problems with much larger sizes of  $15 \times 15$ , while standard diffusion completely fails.

In summary, our contributions are as follows: **(1)** We introduce *Test-time Scalable MCTS-enhanced Diffusion Model* (T-SCEND) as a novel framework that can scale up test-time computation for better reasoning capability. **(2)** We introduce Linear-Regression Negative Contrastive Learning (LRNCL) and KL regularization into the training objective to improve the energy landscape. **(3)** We integrate a hybrid Monte Carlo Tree Search into the denoising process, enabling test-time scaling for better reasoning accuracy. **(4)** We demonstrate the effectiveness of our method on challenging Sudoku and Maze datasets where the conditions are OOD or the problem sizes are much larger.

## 2. Related Work

**Controllable Generation of Diffusion Models:** Controllable generation in diffusion models has been a significant area of research aiming to guide the generation process to produce samples that meet specific criteria or constraints. Previous work focuses on controlling the generation process through an external or internal gradient (Dhariwal & Nichol, 2021; Ho & Salimans, 2021), which requires additional training according to each new objective. T-SCEND does not rely on external guidance/classifiers or conditional training but instead utilizes sampling, simulation, and selection during inference to navigate the generation process.

**Test-time scaling and MCTS:** Test-time scaling involves augmenting computational resources during the inference phase to improve model performance. This approach has gained significant attention in the field of large language models (LLMs) (Brown et al., 2024; Snell et al., 2024; Wu et al., 2024a), substantially enhancing their capabilities. Techniques such as CoT (Wei et al., 2022) and TOT (Yao et al., 2024) are commonly used to incorporate explicit reasoning steps to strengthen the model's reasoning abilities. Monte Carlo Tree Search (MCTS) (Coulom, 2006; Kocsis & Szepesvári, 2006; Gelly et al., 2006) is a heuristic search algorithm designed for decision-making processes. Recently, MCTS has been increasingly integrated with deep learning, particularly reinforcement learning, providing an efficient

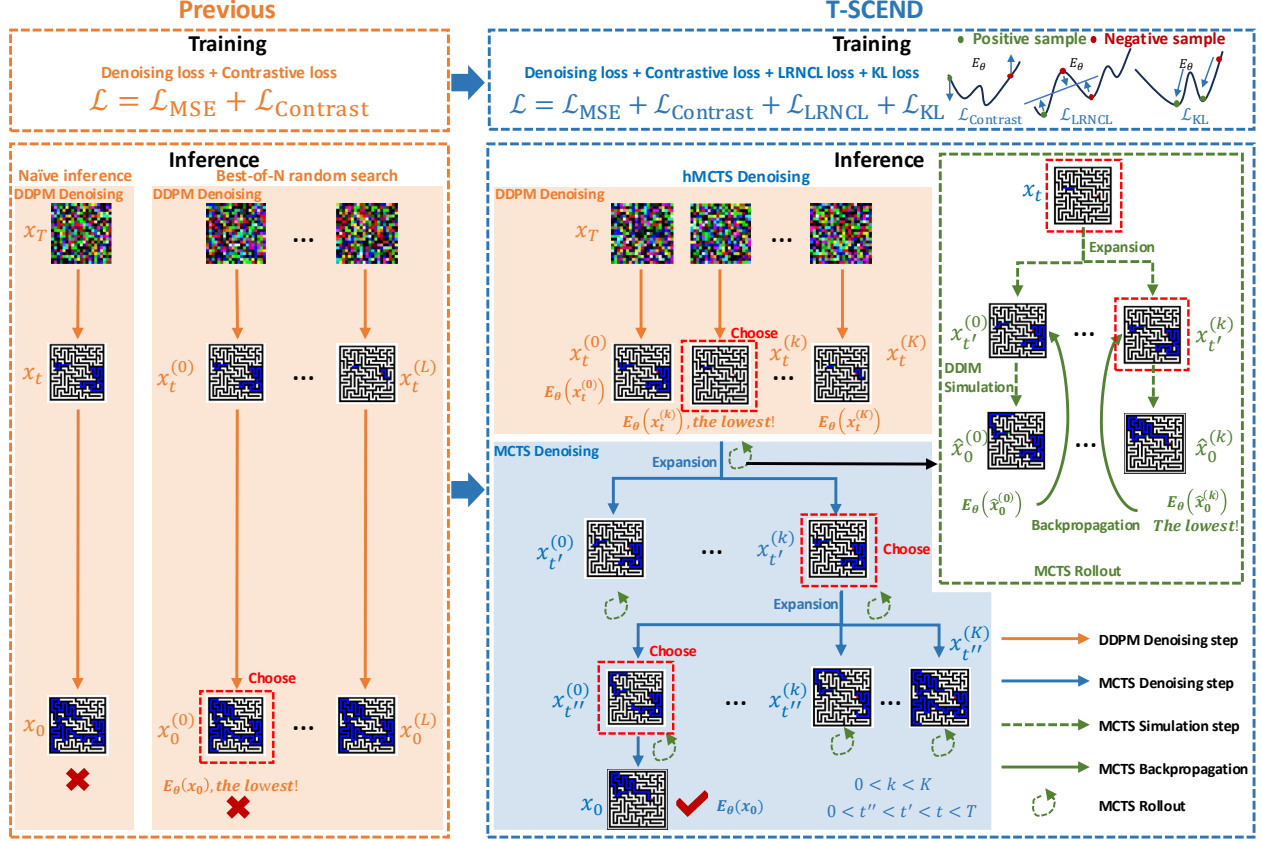


Figure 2. Overview of T-SCEND. This figure illustrates the key aspects of T-SCEND by contrasting its training and inference strategies with those of the previous method. Specifically, T-SCEND introduces  $\mathcal{L}_{\text{LRNCL}}$  and  $\mathcal{L}_{\text{KL}}$  during training and incorporates Monte Carlo Tree Search (MCTS) during inference to enable efficient scaling.

means of enhancing computational search during inference (Silver et al., 2016; 2017; 2018; Schrittwieser et al., 2020).

The idea of test-time scaling for diffusion models was concurrently explored by Ma et al. (2025). Their approach investigates how test-time computation budgets affect scaling performance, as well as the influence of different verifiers and scaling search algorithms. In contrast, we focus on why naïvely trained diffusion models fail and propose KL loss and LRNCL loss to enhance the diffusion model’s capacity, facilitating better scalability. For test-time scaling methods, we introduce hMCTS denoising, which innovatively integrates MCTS and the denoising process to fully unlock the scalability of the diffusion model.

### 3. Preliminary

The Denoising Diffusion Probabilistic Model (DDPM) (Ho et al., 2020) contains a predefined forward process to corrupt data into Gaussian noises, and a learnable reverse process to generate new samples from them. The forward process follows a Gaussian transition kernel  $q(\mathbf{x}_t|\mathbf{x}_{t-1}) = \mathcal{N}(\mathbf{x}_t|\sqrt{\alpha_t}\mathbf{x}_{t-1}, (1-\alpha_t)\mathbf{I})$ ,  $t = 1, \dots, T$ , where the noise

schedule  $\{\alpha_t\}_{t=1}^T$  and  $T$  is set to make  $\mathbf{x}_T$  follow approximately a standard Gaussian distribution. The reverse process can be learned to predict the noise from the corrupted data by minimizing

$$\mathcal{L}_{\text{MSE}} = \mathbb{E}_{\mathbf{x}_0, \epsilon, t} \left[ \left\| \epsilon - \epsilon_\theta \left( \sqrt{\alpha_t} \mathbf{x}_0 + \sqrt{1 - \alpha_t} \epsilon, t \right) \right\|_2^2 \right], \quad (1)$$

where the expectation is w.r.t.  $\mathbf{x}_0 \sim p(\mathbf{x})$ ,  $\epsilon \sim \mathcal{N}(\mathbf{0}, \mathbf{I})$ , and  $t \sim \{1, \dots, T\}$ .  $\bar{\alpha}_t := \prod_{i=1}^t \alpha_i$ . Eq. 1 is equivalent to optimizing a reweighted variational bound on negative log-likelihood. Without loss of generality, in this work, we parameterize  $\epsilon_\theta$  as the gradient of the energy function  $\nabla_{\mathbf{x}_t} E_\theta(\mathbf{x}_t, t)$  as in Du et al. (2023)<sup>4</sup>. To improve the energy landscape, Du et al. (2024) introduced a contrastive loss

$$\mathcal{L}_{\text{Contrast}} = \mathbb{E}_{\mathbf{x}_0, \mathbf{x}_0^-, \epsilon, t} \left[ -\log \left( \frac{e^{-E_\theta(\mathbf{x}_t, t)}}{e^{-E_\theta(\mathbf{x}_t, t)} + e^{-E_\theta(\mathbf{x}_t^-, t)}} \right) \right], \quad (2)$$

<sup>4</sup>This parameterization has the benefit that it simultaneously learns  $\epsilon_\theta$  as gradient of the energy  $\nabla_{\mathbf{x}_t} E_\theta(\mathbf{x}_t, t)$  and learns the energy itself as an unnormalized log-probability due to  $p(\mathbf{x}_t) \propto e^{-E_\theta(\mathbf{x}_t, t)}$ , allowing inference to utilize this “energy” as guidance.

where  $\mathbf{x}_0 \sim p(\mathbf{x})$ ,  $\boldsymbol{\epsilon} \sim \mathcal{N}(\mathbf{0}, \mathbf{I})$ ,  $\mathbf{x}_t = \sqrt{\bar{\alpha}_t}\mathbf{x}_0 + \sqrt{1 - \bar{\alpha}_t}\boldsymbol{\epsilon}$ .  $\mathbf{x}_t^- = \sqrt{\bar{\alpha}_t}\mathbf{x}_0^- + \sqrt{1 - \bar{\alpha}_t}\boldsymbol{\epsilon}$ . Here  $\mathbf{x}_0^- \sim p_{\text{corrupt}}(\mathbf{x}_0^- | \mathbf{x}_0)$  are negative examples by corrupting the positive examples  $\mathbf{x}_0$ . This contrastive loss encourages the positive (ground-truth) examples to have global energy minima.

The reverse process starts with  $\mathbf{x}_T \sim \mathcal{N}(\mathbf{0}, \mathbf{I})$ , and iteratively applies the learned denoising net  $\epsilon_\theta$ , where Song et al. introduces an adjustable noise scale  $\sigma_t$ :

$$\begin{aligned} \mathbf{x}_{t-1} &= \frac{\sqrt{\bar{\alpha}_{t-1}}\mathbf{x}_t - \sqrt{1 - \bar{\alpha}_t}\epsilon_\theta(\mathbf{x}_t, t)}{\sqrt{\bar{\alpha}_t}} \\ &+ \sqrt{1 - \bar{\alpha}_{t-1} - \sigma_t^2}\epsilon_\theta(\mathbf{x}_t, t) + \sigma_t\boldsymbol{\epsilon}_t, \quad \boldsymbol{\epsilon}_t \sim \mathcal{N}(\mathbf{0}, \mathbf{I}) \end{aligned} \quad (3)$$

Importantly, Song et al. highlights that a diffusion model trained with  $\{\alpha_t\}_{t=1}^T$  can be used to sample with  $\{\alpha_{\tau_s}\}_{s=1}^S$ , where  $\tau$  is any increasing sub-sequence of  $1, 2, \dots, T$  of length  $S$ , which significantly accelerates sampling, and will serve as an efficient approach for MCTS simulation in Section 4.3.

## 4. Method

### 4.1. Problem setup

Consider an optimization problem  $\min_{\mathbf{x} \in \mathcal{C}} \mathcal{J}(\mathbf{x})$  with objective  $\mathcal{J} : \mathbb{R}^n \rightarrow \mathbb{R}$  and feasible set  $\mathcal{C} \subseteq \mathbb{R}^n$ . We focus on cases where  $\mathbb{R}^n$  is a high-dimensional space and a dataset  $\{\mathbf{x}_i\}$  drawn from  $p(\mathbf{x})$  supported on  $\mathcal{C}$  is given. The dataset has two-fold effects here. First, in real-world applications, the explicit expression of  $\mathcal{C}$  is often unavailable, and can only be learned implicitly from samples. Second, in high-dimensional problems, data prior could make the search much more efficient, as we will demonstrate in Section 5.

### 4.2. Training of T-SCEND

Although the denoising loss  $\mathcal{L}_{\text{MSE}}$  (Eq. 1) and the contrastive loss  $\mathcal{L}_{\text{Contrast}}$  (Eq. 2) are effective, we find that simply scaling up inference budget by having more independent random search processes yields marginal gain (Sec. 5.1). Through deeper analysis, we find that the core reason is insufficient *performance-energy consistency* and *adversarial sampling*, which we address by introducing a novel Linear-Regression Negative Contrastive Learning loss and incorporating a KL regularization, which we detail as follows.

**Linear-Regression Negative Contrastive Learning.** Concretely, although the contrastive loss (Eq. 2) encourages the positive examples to have global minimum energy, it does not stipulate the landscape for the negative examples. For example, it is likely that a negative example  $\mathbf{x}_t^{--}$  that is further apart from the positive example  $\mathbf{x}_t$  has lower energy than a negative example  $\mathbf{x}_t^-$  that is nearer. Thus, the inference process can start around  $\mathbf{x}_t^{--}$  and can hardly move

out. This will result in reduced *performance-energy consistency*, where lower energy at step  $t$  does not necessarily correspond to a more accurate predicted solution  $\hat{\mathbf{x}}_0$ , as will be shown in Sec. 5.1. This problem can not be easily remedied by having more inference budget such as more random search processes. A more fundamental way to solve this problem is to shape the energy landscape by regularizing the energy *among* negative examples during *training*. Specifically, from a positive example  $\mathbf{x}_0 \sim p(\mathbf{x})$ , we sample two negative examples  $\mathbf{x}_0^-$  and  $\mathbf{x}_0^{--}$ <sup>5</sup>, the latter has a larger L2 distance to  $\mathbf{x}_0$ . Specifically, the distance of  $\mathbf{x}_0$ ,  $\mathbf{x}_0^-$  and  $\mathbf{x}_0^{--}$  to  $\mathbf{x}_0$  are 0,  $l_{2,0}^- = \|\mathbf{x}_0^- - \mathbf{x}_0\|_2^2$ , and  $l_{2,0}^{--} = \|\mathbf{x}_0^{--} - \mathbf{x}_0\|_2^2$ , respectively. Then we obtain their corresponding noisy examples at step  $t$  via  $\mathbf{x}_t = \sqrt{\bar{\alpha}_t}\mathbf{x}_0 + \sqrt{1 - \bar{\alpha}_t}\boldsymbol{\epsilon}$ ,  $\mathbf{x}_t^- = \sqrt{\bar{\alpha}_t}\mathbf{x}_0^- + \sqrt{1 - \bar{\alpha}_t}\boldsymbol{\epsilon}$ , and  $\mathbf{x}_t^{--} = \sqrt{\bar{\alpha}_t}\mathbf{x}_0^{--} + \sqrt{1 - \bar{\alpha}_t}\boldsymbol{\epsilon}$ . Their energy are  $E_t^+ = E_\theta(\mathbf{x}_t, t)$ ,  $E_t^- = E_\theta(\mathbf{x}_t^-, t)$ , and  $E_t^{--} = E_\theta(\mathbf{x}_t^{--}, t)$ , respectively. To encourage a landscape where the energy difference between negative samples and the positive sample becomes smaller as they approach the positive sample, we directly constrain the relationship between the energy of different negative samples and the positive sample using linear regression. Specifically, we first apply the linear regression algorithm<sup>6</sup> to fit a line through the three points  $\{(0, E_t^+), (l_{2,0}^-, E_t^-), (l_{2,0}^{--}, E_t^{--})\}$ , which is characterized by the slope  $k_t$  and the intercept  $b_t$ . Then, we obtain the corresponding fitted points  $\{(0, \hat{E}_t^+), (l_{2,0}^-, \hat{E}_t^-), (l_{2,0}^{--}, \hat{E}_t^{--})\}$ . We then compute the Linear-Regression Negative Contrastive Learning (LRNCL) loss as follows:

$$\begin{aligned} \mathcal{L}_{\text{LRNCL}} &= \mathbb{E}_{\mathbf{x}_0, \mathbf{x}_0^-, \mathbf{x}_0^{--}, \boldsymbol{\epsilon}, t} [\max(0, \gamma - k_t) + \\ &\|E_t^+ - \hat{E}_t^+\|_2^2 + \|E_t^- - \hat{E}_t^-\|_2^2 + \|E_t^{--} - \hat{E}_t^{--}\|_2^2], \end{aligned} \quad (4)$$

where  $\gamma$  is a hyperparameter and  $t \sim \{0, \dots, T\}$ . The first term  $\max(0, \gamma - k_t)$  encourages that any three samples  $\mathbf{x}_t$ ,  $\mathbf{x}_t^-$ ,  $\mathbf{x}_t^{--}$  have a positive (and larger-than- $\gamma$ ) slope of energy vs. L2 distance. The latter three terms encourage that the energy vs. L2 distance is linear, making the energy landscape more smooth<sup>7</sup>.

**KL regularization.** Besides *performance-energy consistency*, another important challenge preventing better test-time scaling is *adversarial sampling*. Specifically, during training, the contrastive loss such as Eq. 2 often leads to *adversarial sampling* where the energy function learns to simply generate an energy landscape that makes sampling difficult. To address this issue, we incorporate the

<sup>5</sup>Details to generate negative samples are in Appendix A.

<sup>6</sup>The details of linear regression algorithm can be found in Appendix A.

<sup>7</sup>It is also possible to use more complex shapes than linear regression to regularize the energy landscape, which we leave for future work. Here we find that simple linear regression works well.

KL-regularization as in Du et al. (2021):

$$\mathcal{L}_{\text{KL}} = \mathbb{E}_{t, p_{\theta, t}(\mathbf{x})} [E_{\text{stop-grad}(\theta)}(\mathbf{x})] + \mathbb{E}_{t, p_{\theta, t}(\mathbf{x})} [\log p_{\theta, t}(\mathbf{x})] \quad (5)$$

where  $p_{\theta, t}(\mathbf{x})$  is the probability distribution of  $\mathbf{x}_t$  at denoising step  $t$ . When optimizing w.r.t.  $\mathcal{L}_{\text{KL}}$ , it is essentially optimizing w.r.t. the sampling (denoising) process by shaping the energy landscape to make it easier to sample. The first term in  $\mathcal{L}_{\text{KL}}$  encourages the samples  $\mathbf{x}_t$  to have low energy, and the second term is maximizing the entropy of the samples, encouraging the samples to be diverse. Both terms allow better test-time scaling. Different from Du et al. (2021), we have this KL regularization on each denoising step  $t$ , and we employ a more accurate estimation of the entropy (Lombardi & Pant, 2016).

Taken together, the training objective of our T-SCEND is:

$$\mathcal{L} = \mathcal{L}_{\text{MSE}} + \mathcal{L}_{\text{Contrast}} + \mathcal{L}_{\text{LRNCL}} + \mathcal{L}_{\text{KL}}, \quad (6)$$

where the latter two terms improve the energy landscape and boost the test-time scalability of diffusion models.

### 4.3. Inference of T-SCEND

To fully harness the potential of the diffusion model, we propose a novel hybrid Monte Carlo Tree Search denoising (hMCTS denoising) method, which progressively applies random search and Monte Carlo Tree Search (MCTS) denoising in sequence, as detailed below, throughout the denoising process. As demonstrated in Algorithm 1, we employ the best-of-N random search for the diffusion process in the early diffusion stages, which introduces  $L$  initial noises to maintain a consistent number of function evaluations (NFE) per example during the diffusion process<sup>8</sup>. Subsequently, hMCTS denoising utilizes the MCTS denoising<sup>9</sup> to iteratively perform the denoising process until the termination state  $\mathbf{x}_0$  is reached. This approach enables MCTS to more accurately estimate node value when the noise is relatively small, thereby preventing the premature exclusion of potentially promising nodes. Next, we will detail the MCTS denoise process.

We treat the current diffusion state  $\mathbf{x}_t$  as the state, the noise to remove as the action, and model the denoising process of the diffusion model as a Markov Decision Process (MDP). Therefore, a *node* in MCTS represents the state  $\mathbf{x}_t$ , along with its current visit count  $N(\mathbf{x}_t)$  and state value  $Q(\mathbf{x}_t)$ . A terminal node is defined as a node whose denoising step is 0. In this context, we use  $\nabla_{\mathbf{x}_t} E_{\theta}(\mathbf{x}_t, t)$  and  $E_{\theta}(\mathbf{x}_t, t)$  of

<sup>8</sup>In this paper, we primarily report  $K = N_r$  MCTS denoising, where ensuring  $K = N_r$ ,  $L = N_r$  guarantees that the NFE (Number of Function Evaluations) for each case of best-of-N random search, MCTS denoising, and hMCTS denoising remains the same.

<sup>9</sup>For a detailed explanation of the distinctions between hMCTS denoising, MCTS denoising, and best-of-N random search, as well as the impact of MCTS denoising start step  $t_s$ , please refer to Appendix D.

the energy-based diffusion as the policy network and value network, respectively. Each deepening of the search tree corresponds to a single denoising step. Similar to MCTS in AlphaGo (Silver et al., 2016) and AlphaZero (Silver et al., 2017), each rollout in MCTS consists of four core steps: selection, expansion, simulation, and backpropagation, as illustrated in Fig. 2 and Algorithm 1:

**(1) Selection:** Based on the Upper Confidence Bound (UCB) from AlphaGo (Silver et al., 2016):

$$UCB(s, a) = Q(s, a) + cP(s, a) \sqrt{\frac{\sum_b N(s, b)}{1 + N(s, a)}}, \quad (7)$$

starting from the current root node state  $\mathbf{x}_t$ , we select a child node based on the following adjusted UCB of MCTS-enhanced diffusion formula until a leaf node  $\{\mathbf{x}_{t'}, Q(\mathbf{x}_{t'}), N(\mathbf{x}_{t'})\}$  is reached:

$$UCB(\mathbf{x}_t, \mathbf{a}_t) = Q(\mathbf{x}_t, \mathbf{a}_t) + c \sqrt{\frac{\ln N_i}{n_i}}, \quad (8)$$

where  $Q(\mathbf{x}_t, \mathbf{a}_t)$  represent the value of children node, action  $\mathbf{a}_t$  includes predicted noise  $\epsilon_{\theta}$  and random Gaussian noise  $\epsilon$ ,  $n_i$  represents the number of visits to node  $i$ ,  $N_i$  represents the number of visits to the parent node of  $i$ , and  $c$  is the exploration hyperparameter.

**(2) Expansion:** Unless the state of the node reached is a terminal state  $\mathbf{x}_0$ , we expand the children of the selected node by choosing an action and creating new nodes based on the action. For the expansion step of MCTS denoising, we perform a denoising step and add different but limited Gaussian noise. This results in  $K$  distinct branches  $\{\mathbf{x}_{t'-1}^{(k)} \mid k = 0, 1, \dots, K-1\}$ , where each child node  $\mathbf{x}_{t'-1}^{(k)}$  is derived as following equation adjusted from Eq. 3 :

$$\mathbf{x}_{t'-1}^{(k)} = \frac{\sqrt{\bar{\alpha}_{t'-1}} \mathbf{x}_{t'} - \sqrt{1 - \bar{\alpha}_{t'}} \epsilon_{\theta}(\mathbf{x}_{t'}, t')}{\sqrt{\bar{\alpha}_{t'}}} + \sqrt{1 - \bar{\alpha}_{t'-1} - \sigma_{t'}^2} \epsilon_{\theta}(\mathbf{x}_{t'}, t') + \sigma_{t'} \epsilon^{(k)}, \quad (9)$$

with  $\epsilon_{\theta}(\mathbf{x}_{t'}, t')$  determined by  $\mathbf{x}_{t'}$  and  $t'$ , and  $\epsilon^{(k)} \sim \mathcal{N}(\mathbf{0}, \mathbf{I})$  representing random Gaussian noise.

**(3) Simulation:** We randomly select a child node and perform a random simulation of the MDP until reaching a terminal state. For the simulation of MCTS denoising, we use DDIMs (Song et al.) for fast sampling to obtain  $\hat{\mathbf{x}}_0(\mathbf{x}_{t'-1}^{(k*)})$  from the randomly chosen child node state  $\mathbf{x}_{t'-1}^{(k*)}$ , and then use  $E_{\theta}(\hat{\mathbf{x}}_0(\mathbf{x}_{t'-1}^{(k*)}))$  as the reward for backpropagation.

**(4) Backpropagation:** Finally, we backpropagate the node values to the root node, updating the value of each node using the expected value along the path.

After  $N_r$  rollouts, we select  $\mathbf{x}_{t-1}^{(k)}$  with the largest value

**Algorithm 1** hMCTS denoising of T-SCEND

---

```

1: Input: EBM  $E_\theta(\cdot)$ , Diffusion Steps  $T$ , MCTS
   denoising start step  $t_s$ , Number of initial noise
   of Best-of-N random search  $L$ , Maximum MCTS
   branch count  $K$ , Maximum MCTS rollout step
    $N_r$ , A set of initial diffusion state  $\{\mathbf{x}_T^{(k)} \mid k =$ 
    $1, \dots, L\}$  sampled from Gaussian noise.
2: // Random search for  $T \rightarrow t_s$ 
3: for  $t = T$  to  $t_s$  do
4:   Use Eq. 3 to get  $\mathbf{x}_{t-1}^{(k)}$  for  $k = 1, \dots, L$ 
5: end for
    $\mathbf{x}_{t_s} \leftarrow \arg \min_{\mathbf{x}_{t_s}^{(k)}} E_\theta(\mathbf{x}_{t_s}^{(k)})$ 
6: // MCTS denoising for  $t_s \rightarrow 1$ 
7: for  $t = t_s$  to 1 do
8:   // Do MCTS Rollouts:
9:   for  $i = 1$  to  $N_r$  do
10:    Selection: Use UCB from Eq. 8 to select
      the child node until a leaf node or a terminal
      node  $\{\mathbf{x}_{t'}, Q(\mathbf{x}_{t'}), N(\mathbf{x}_{t'})\}$  is reached and
      form a path using the nodes accessed during
      the selection;
11:    Expansion: Use Eq. 9 to generate child
      node state  $\mathbf{x}_{t'-1}^{(k)}$  for  $\mathbf{x}_{t'}$  and initialize
       $Q(\mathbf{x}_{t'-1}^{(k)}) = 0$ ,  $N(\mathbf{x}_{t'-1}^{(k)}) = 0$  for  $k =$ 
       $0, \dots, K - 1$ ;
12:    Simulation: Randomly choose  $k^* \sim$ 
       $\{0, \dots, K - 1\}$  and do DDIM simulation from
       $\mathbf{x}_{t'-1}^{(k^*)}$  to get  $\hat{\mathbf{x}}_0(\mathbf{x}_{t'-1}^{(k^*)})$ ;
13:    Backpropagation: Update the value and
      visit count of each node  $\mathbf{x}_{t_p}$  in the path using
       $Q(\mathbf{x}_{t_p}) \leftarrow Q(\mathbf{x}_{t_p}) - E_\theta(\hat{\mathbf{x}}_0(\mathbf{x}_{t'-1}^{(k^*)}))$ ;
       $N(\mathbf{x}_{t_p}) \leftarrow N(\mathbf{x}_{t_p}) + 1$ ;
14:    end for
15:     $\mathbf{x}_{t-1} \leftarrow \arg \max_{\mathbf{x}_{t-1}^{(k)}} \frac{Q(\mathbf{x}_{t-1}^{(k)})}{N(\mathbf{x}_{t-1}^{(k)})}$ 
16:  end for
17: return  $\mathbf{x}_0$ 

```

---

$\frac{Q(\mathbf{x}_{t-1}^{(k)})}{N(\mathbf{x}_{t-1}^{(k)})}$  as the state  $\mathbf{x}_{t-1}$  for the next denoising step. The next MCTS denoising process starts from this state and proceeds until the termination state  $\mathbf{x}_0$ . Here, the depth of the search tree is decided by three elements: the number of rollout steps  $N_r$ , the maximum number of branches  $K$  for each node, and the search policy.

To summarize, our proposed paradigm, T-SCEND, enhances *performance-energy consistency* and ease of sampling through LRNCL loss and KL regularization, respectively (Sec. 4.2), while fully unlocking the test-time scalability of diffusion models via hMCTS denoising (Sec. 4.3).

## 5. Experiments

In the experiments, we aim to answer the following questions: (1) What factors contribute to the failure of the direct scaling-up diffusion model? (2) Does the training of T-SCEND unleash the test-time scalability of diffusion model? (3) Can the inference method of T-SCEND effectively achieve scaling up during test time? To answer these questions, we conduct extensive experiments on two challenging reasoning tasks: Maze and Sudoku. In Section 5.1, we find that the naïvely trained diffusion model falls short of scaling up during test time and identify the key reasons as insufficient *performance-energy consistency* and *adversarial sampling*. To address these challenges, the training methods of T-SCEND demonstrate a significant impact on unbinding the scalability of the diffusion model in Section 5.2. As shown in Fig 1, with the model trained with T-SCEND training methods, hMCTS denoising can better release the scalability enabling generalization to much more challenging tasks during inference (Sec. 5.3).

In Maze experiments, the datasets are generated by Ivanitskiy et al. (2023), and the diffusion model is mainly trained with Maze sizes of up to  $6 \times 6$  while tested on harder datasets with size significantly larger than  $6 \times 6$  (Fig. 1). For Sudoku experiments, the basic setting is adopted from Du et al. (2024) where the diffusion model is trained on SAT-Net dataset with 31 to 42 given entries (Wang et al., 2019) and tested on harder RRN dataset with 17 to 34 given entries (Palm et al., 2018) with fewer given entries. All models and inference methods are evaluated with solving success rate. For Maze, successful solving means finding a continuous path from starting location to target location without any breaking or overlapping with the wall; for Sudoku, successful solving means filling all the missing numbers that *exactly* match the ground-truth, both of which are very stringent metrics. More experimental details, hyperparameter analysis, and result visualizations can be found in Appendix B, Appendix C, and Appendix F, respectively. All the training methods are compared with the original training pipeline in Du et al. (2024). LRNCL and KL represent the loss terms  $\mathcal{L}_{\text{LRNCL}}$  and  $\mathcal{L}_{\text{KL}}$ , respectively in Eq. 6. T-SCEND tr. w/o LRNCL, T-SCEND tr. w/o KL, and T-SCEND tr. (ours) represent the three training methods of T-SCEND, the last one being the full version. The MCTS denoising and hMCTS denoising are primarily compared with the best-of-N random search with the same computational budget.

### 5.1. Why originally trained model fail to scale up during test time?

To investigate why diffusion models trained via the original method fail on more complex tasks, even with increased inference budgets yielding minimal improvement, we evaluate models trained on simpler datasets against harder tasks.

Table 1. Success rate across different grid sizes of Maze and various number of given entries for naive inference ( $N = 1$ ) for comparison of the generalization ability of models obtained by different training methods. Let  $M$  denotes the grid size of Maze and  $D$  denotes the number of given digits in Sudoku. Original denotes the original training method in Du et al. (2024). T-SCEND tr. (ours) denotes the training method of T-SCEND, and all subsequent descriptions will follow this definition. Bold font denotes the best model, and underline denotes the second best model. The same markings are used in the tables below.

Methods	Maze success rate					Sudoku success rate				
	$M = 6$	$M = 8$	$M = 10$	$M = 12$	$M = 15$	$D = 33$	$D = 29$	$D = 25$	$D = 21$	$D = 17$
Original	1.0000	0.9062	0.5781	0.3750	0.0625	0.3203	0.1094	0.0234	0.0000	0.0000
T-SCEND tr. w/o LRNCL	1.0000	0.9922	<u>0.7734</u>	<u>0.5625</u>	0.2500	<b>0.4219</b>	<u>0.1719</u>	<b>0.0469</b>	<b>0.0078</b>	0.0000
T-SCEND tr. w/o KL	1.0000	0.9844	0.6953	0.4375	<u>0.2812</u>	<b>0.4219</b>	<b>0.2578</b>	<u>0.0391</u>	<b>0.0078</b>	0.0000
T-SCEND tr. (ours)	1.0000	<b>1.0000</b>	<b>0.9922</b>	<b>0.9141</b>	<b>0.6562</b>	0.1953	0.1016	0.0078	0.0000	0.0000

Table 2. Success rate on Maze with grid size 15 and Sudoku harder dataset for comparison of the model’s ability to scale up under random search with different training methods. Here,  $N_r = N, K = N, L = N$ .

Methods	Maze success rate						Sudoku success rate						
	$N=1$	$N=11$	$N=21$	$N=41$	$N=81$	$N=161$	$N=1$	$N=11$	$N=21$	$N=41$	$N=81$	$N=161$	$N=321$
Original, Random search	0.0625	0.0469	0.0547	0.0781	0.1016	0.1094	0.0859	0.1641	0.2188	0.2344	0.2422	0.2656	0.2812
T-SCEND tr. w/o LRNCL, Random search	0.2500	0.4297	<u>0.5000</u>	0.5391	<u>0.6016</u>	0.6094	<u>0.1172</u>	<b>0.2656</b>	<u>0.3125</u>	<b>0.3438</b>	<b>0.3750</b>	<b>0.3906</b>	<b>0.4141</b>
T-SCEND tr. w/o KL, Random search	<b>0.2812</b>	<u>0.4688</u>	0.4922	<u>0.5547</u>	0.5859	<u>0.6250</u>	<b>0.1562</b>	0.2422	0.2578	0.2656	0.2656	0.2891	0.3047
T-SCEND tr. (ours), Random search	<u>0.2656</u>	<b>0.5859</b>	<b>0.6406</b>	<b>0.6875</b>	<b>0.6562</b>	<b>0.7031</b>	0.0703	<u>0.2500</u>	<b>0.3281</b>	<b>0.3438</b>	<u>0.3516</u>	<u>0.3594</u>	<u>0.3906</u>

Table 3. Performance-energy consistency of random search on Maze with grid size 15 and Sudoku harder dataset to test the effect of LRNCL loss. Here,  $L = N$ . Details of consistency calculation can be found in Appendix A.

Methods	Maze performance-energy consistency					Sudoku Performance-energy consistency				
	$N=11$	$N=21$	$N=41$	$N=81$	$N=161$	$N=11$	$N=21$	$N=41$	$N=81$	$N=161$
Original, Random search	0.3094	0.2916	0.3129	0.3143	0.3103	0.3955	0.3930	0.4010	0.4010	0.3986
T-SCEND tr. w/o KL, Random search	<b>0.5375</b>	<b>0.4316</b>	<b>0.4902</b>	<b>0.5006</b>	<b>0.4998</b>	<b>0.4574</b>	<b>0.4528</b>	<b>0.4457</b>	<b>0.4459</b>	<b>0.4470</b>

As shown in Table 1, models trained on simpler tasks with original training methods exhibit significantly poorer performance on more complex tasks. For the Maze task, models trained on maze sizes of  $4 \times 4$ ,  $5 \times 5$ , and  $6 \times 6$  demonstrate a rapid decline in success rate as the maze size increases. Specifically, the success rate decreases from 100% at  $6 \times 6$  to 6% at  $15 \times 15$ . A similar trend is observed in the Sudoku task: models trained on datasets with 31 to 42 given entries fail to achieve high success rates when tested on datasets with 17 to 34 given entries, with the success rate dropping to below 5% when the number of entries is reduced to 25, and complete failure when only 21 entries are provided.

Building upon this, we conduct best-of- $N$  random search to examine whether test-time scaling can enhance the performance of the originally trained model, as described in Section 4.3, and the results are presented in Table 2 and Table 3. In Table 2, it is evident that, for the originally trained model, increasing the inference budget  $N$  in the Maze experiment only yields a modest improvement, with the success rate increasing by at most 5%, reaching a peak of 10%. In the Sudoku experiment, even with an increased budget of  $N = 320$ , the success rate remains below 30%. The results in Table 3 further reveal that the energy model predictions of the originally trained model exhibit substantial misalignment with true performance metrics, with many good samples assigned higher energy values. In the Maze experiment, the consistency between the energy model and true perfor-

mance is only 30% while the consistency in Sudoku task is around 40%. These results indicate that the originally trained model suffers from insufficient *performance-energy consistency*. Additionally, as seen in Table 10, even when ground truth is used to evaluate multiple candidates generated via random search with the originally trained model, the model’s performance remains unsatisfactory, with the Maze success rate not exceeding 20% and the Sudoku success rate below 30%. This result demonstrates that the originally trained model is affected by *adversarial sampling*. Even with an increased computation budget  $N$ , the generated samples remain suboptimal or correspond to incorrect global optima, hindering the acquisition of high-quality samples that align with the correct global optimum.

### 5.2. The effect of T-SCEND training methods

To enhance the *performance-energy consistency* and reduce *adversarial sampling*, as detailed in 4.2, we augmented the originally trained method with additional LRNCL loss and KL loss. As shown in Table 3, incorporating LRNCL loss into the training process significantly improves the *performance-energy consistency* compared to the original model, with a greater than 20% improvement in the Maze task and a 5% improvement in the Sudoku task. In Table 2, for the Maze task, even without any additional computation (*i.e.*,  $N = 1$ ), models trained with KL loss achieve a 20% increase in solving success rate compared to the

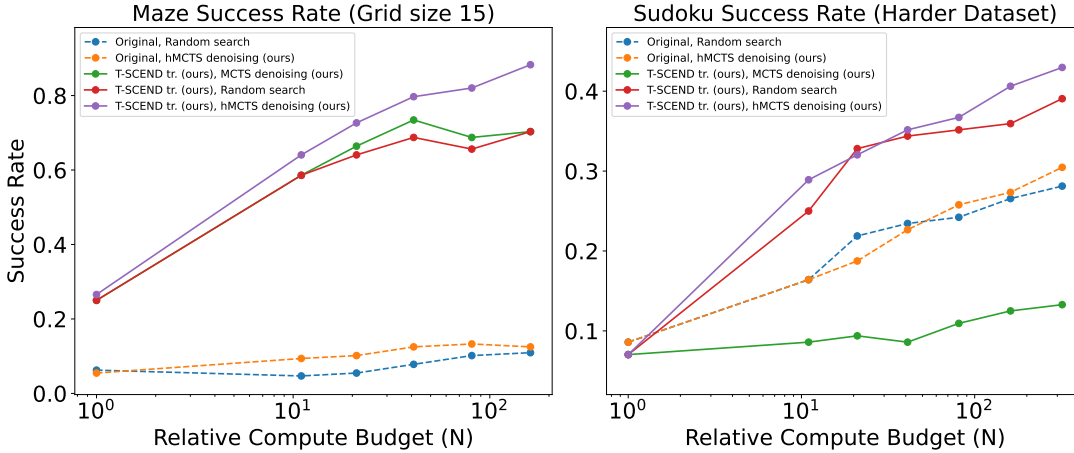


Figure 3. Scalability of different approaches on Maze and Sudoku.

Table 4. Success rate of different approaches on Maze with grid size 15 and Sudoku harder dataset. Here,  $N_r = N, K = N, L = N$ .

Methods	Maze success rate						Sudoku success rate						
	$N=1$	$N=11$	$N=21$	$N=41$	$N=81$	$N=161$	$N=1$	$N=11$	$N=21$	$N=41$	$N=81$	$N=161$	$N=321$
Original, Random search	0.0625	0.0469	0.0547	0.0781	0.1016	0.1094	<b>0.0859</b>	0.1641	0.2188	0.2344	0.2422	0.2656	0.2812
Original, hMCTS denoising (ours)	0.0625	0.0938	0.1016	0.1250	0.1328	0.1250	<b>0.0859</b>	0.1641	0.1875	0.2266	0.2578	0.2734	0.3047
T-SCEND tr. (ours), MCTS denoising (ours)	0.2656	0.5859	<u>0.6641</u>	<u>0.7344</u>	<u>0.6875</u>	0.7031	<u>0.0703</u>	0.0859	0.0938	0.0859	0.1094	0.1250	0.1328
T-SCEND tr. (ours), Random search	0.2656	0.5859	0.6406	0.6875	0.6562	0.7031	<u>0.0703</u>	<u>0.2500</u>	<b>0.3281</b>	<u>0.3438</u>	<u>0.3516</u>	<u>0.3594</u>	<u>0.3906</u>
T-SCEND tr. (ours), hMCTS denoising (ours)	<b>0.2656</b>	<b>0.6406</b>	<b>0.7266</b>	<b>0.7969</b>	<b>0.8203</b>	<b>0.8828</b>	<u>0.0703</u>	<b>0.2891</b>	<u>0.3203</u>	<b>0.3516</b>	<b>0.3672</b>	<b>0.4062</b>	<b>0.4297</b>

original model. Models trained with LRNCL loss show an improvement of over 20%. Augmented with random search, as the budget  $N$  increases, the improvement for all three training methods becomes more pronounced. Models trained with KL loss show a maximum success rate increase of approximately 50%, those with LRNCL loss exceed a 50% improvement, and the combination of both KL loss and LRNCL loss results in a maximum increase of about 60%. In the Sudoku task, using the naive inference method with  $N = 1$ , both KL loss and LRNCL loss yield significant improvements. For Random Search, as  $N$  increases, models trained with all three T-SCEND methods surpass the original model at  $N = 21$ , with the gap widening further as the budget grows, showing a maximum increase of over 10%. Furthermore, Table 10 shows that the T-SCEND-trained energy-based diffusion model outperforms DDPM (Ho et al., 2020) under the same architecture. These results demonstrate that the training methods of T-SCEND can effectively improve *performance-energy consistency* and reduce *adversarial sampling* to unlock the test-time scalability of diffusion models.

### 5.3. Test-time Scalability of T-SCEND

Using the diffusion model trained with T-SCEND training methods, we evaluate various inference approaches on the Maze task with a grid size of  $15 \times 15$  and on a more challenging Sudoku dataset. As shown in Table 4, models trained with additional LRNCL loss and KL loss of T-SCEND demonstrate that, in the Maze experiment,

the MCTS denoising method slightly outperforms random search, while our hMCTS denoising yields a significantly higher success rate, with a maximum improvement of approximately 18% than random search. Moreover, as the budget  $N$  increases, the performance gap between hMCTS denoising and random search widens. In the Sudoku experiment, hMCTS denoising also consistently outperforms random search, with a maximum improvement of 5%. As illustrated in the *scaling curve* in Fig. 3, hMCTS denoising with the model trained with additional LRNCL loss and KL loss shows a marked improvement in solving success rate compared to both other inference methods and hMCTS denoising with the originally trained model. At the same time, the rate of improvement in solving success rate for other inference methods clearly slows down compared to hMCTS denoising. These results provide strong evidence that our inference method can effectively scale up during test time, offering a clear advantage over random search.

## 6. Conclusion

In this work, we have introduced *Test-time Scalable MCTS-enhanced Diffusion Model* (T-SCEND), a novel framework that enhances the scalability of diffusion models in testing to tackle more complex tasks than in training. We demonstrate that naive scaling of existing diffusion models yields marginal performance gains. To address this, we introduce two auxiliary training loss,  $\mathcal{L}_{LRNCL}$  and  $\mathcal{L}_{KL}$ , to improve *performance-energy consistency* and reduce *adversarial sampling* while integrating hybrid Monte Carlo Tree Search



(hMCTS) denoising to fully exploit the model’s scalability in inference. We have conducted extensive experiments on Maze and Sudoku to validate the efficacy of our method and believe that T-SCEND offers a robust solution for test-time scaling, unlocking the notable potential of diffusion models. We discuss limitations and future work in Appendix E.

## References

- Brooks, T., Peebles, B., Holmes, C., DePue, W., Guo, Y., Jing, L., Schnurr, D., Taylor, J., Luhman, T., Luhman, E., Ng, C., Wang, R., and Ramesh, A. Video generation models as world simulators. 2024. URL <https://openai.com/research/video-generation-models-as-world-simulators>
- Brown, B., Juravsky, J., Ehrlich, R., Clark, R., Le, Q. V., Ré, C., and Mirhoseini, A. Large language monkeys: Scaling inference compute with repeated sampling. *arXiv preprint arXiv:2407.21787*, 2024.
- Coulom, R. Efficient selectivity and backup operators in monte-carlo tree search. In *International conference on computers and games*, pp. 72–83. Springer, 2006.
- Dhariwal, P. and Nichol, A. Diffusion models beat gans on image synthesis. In Ranzato, M., Beygelzimer, A., Dauphin, Y., Liang, P., and Vaughan, J. W. (eds.), *Advances in Neural Information Processing Systems*, volume 34, pp. 8780–8794. Curran Associates, Inc., 2021. URL [https://proceedings.neurips.cc/paper\\_files/paper/2021/file/49ad23d1ec9fa4bd8d77d02681df5cfa-Paper.pdf](https://proceedings.neurips.cc/paper_files/paper/2021/file/49ad23d1ec9fa4bd8d77d02681df5cfa-Paper.pdf).
- Du, Y., Li, S., Tenenbaum, J., and Mordatch, I. Improved contrastive divergence training of energy-based models. In *International Conference on Machine Learning*, pp. 2837–2848. PMLR, 2021.
- Du, Y., Durkan, C., Strudel, R., Tenenbaum, J. B., Dieleman, S., Fergus, R., Sohl-Dickstein, J., Doucet, A., and Grathwohl, W. S. Reduce, reuse, recycle: Compositional generation with energy-based diffusion models and mcmc. In *International conference on machine learning*, pp. 8489–8510. PMLR, 2023.
- Du, Y., Mao, J., and Tenenbaum, J. B. Learning iterative reasoning through energy diffusion. *arXiv preprint arXiv:2406.11179*, 2024.
- Gelly, S., Wang, Y., Munos, R., and Teytaud, O. *Modification of UCT with Patterns in Monte-Carlo Go*. PhD thesis, INRIA, 2006.
- Ho, J. and Salimans, T. Classifier-free diffusion guidance. In *NeurIPS 2021 Workshop on Deep Generative Models and Downstream Applications*, 2021.
- Ho, J., Jain, A., and Abbeel, P. Denoising diffusion probabilistic models. *Advances in neural information processing systems*, 33:6840–6851, 2020.
- Ivanitskiy, M. I., Shah, R., Spies, A. F., Räucher, T., Valentine, D., Rager, C., Quirke, L., Mathwin, C., Corlouer, G., Behn, C. D., et al. A configurable library for generating and manipulating maze datasets. *arXiv preprint arXiv:2309.10498*, 2023.
- Janner, M., Du, Y., Tenenbaum, J., and Levine, S. Planning with diffusion for flexible behavior synthesis. In *International Conference on Machine Learning*, pp. 9902–9915. PMLR, 2022.
- Karras, T., Aittala, M., Aila, T., and Laine, S. Elucidating the design space of diffusion-based generative models. *Advances in neural information processing systems*, 35: 26565–26577, 2022.
- Kocsis, L. and Szepesvári, C. Bandit based monte-carlo planning. In *European conference on machine learning*, pp. 282–293. Springer, 2006.
- Lane, D., Scott, D., Hebl, M., Guerra, R., Osherson, D., and Zimmer, H. *Introduction to statistics*. Citeseer, 2003.
- Lombardi, D. and Pant, S. Nonparametric k-nearest-neighbor entropy estimator. *Physical Review E*, 93(1): 013310, 2016.
- Ma, N., Tong, S., Jia, H., Hu, H., Su, Y.-C., Zhang, M., Yang, X., Li, Y., Jaakkola, T., Jia, X., and Xie, S. Inference-time scaling for diffusion models beyond scaling denoising steps, 2025. URL <https://arxiv.org/abs/2501.09732>.
- Palm, R., Paquet, U., and Winther, O. Recurrent relational networks. *Advances in neural information processing systems*, 31, 2018.
- Rombach, R., Blattmann, A., Lorenz, D., Esser, P., and Ommer, B. High-resolution image synthesis with latent diffusion models. In *Proceedings of the IEEE/CVF conference on computer vision and pattern recognition*, pp. 10684–10695, 2022.
- Schrittwieser, J., Antonoglou, I., Hubert, T., Simonyan, K., Sifre, L., Schmitt, S., Guez, A., Lockhart, E., Hassabis, D., Graepel, T., et al. Mastering atari, go, chess and shogi by planning with a learned model. *Nature*, 588(7839): 604–609, 2020.
- Silver, D., Huang, A., Maddison, C. J., Guez, A., Sifre, L., Van Den Driessche, G., Schrittwieser, J., Antonoglou, I., Panneershelvam, V., Lanctot, M., et al. Mastering the game of go with deep neural networks and tree search. *nature*, 529(7587):484–489, 2016.

- Silver, D., Schrittwieser, J., Simonyan, K., Antonoglou, I., Huang, A., Guez, A., Hubert, T., Baker, L., Lai, M., Bolton, A., et al. Mastering the game of go without human knowledge. *nature*, 550(7676):354–359, 2017.
- Silver, D., Hubert, T., Schrittwieser, J., Antonoglou, I., Lai, M., Guez, A., Lanctot, M., Sifre, L., Kumaran, D., Graepel, T., et al. A general reinforcement learning algorithm that masters chess, shogi, and go through self-play. *Science*, 362(6419):1140–1144, 2018.
- Snell, C., Lee, J., Xu, K., and Kumar, A. Scaling llm test-time compute optimally can be more effective than scaling model parameters. *arXiv preprint arXiv:2408.03314*, 2024.
- Sohl-Dickstein, J., Weiss, E., Maheswaranathan, N., and Ganguli, S. Deep unsupervised learning using nonequilibrium thermodynamics. In *International conference on machine learning*, pp. 2256–2265. PMLR, 2015.
- Song, J., Meng, C., and Ermon, S. Denoising diffusion implicit models. In *International Conference on Learning Representations*.
- Song, Y., Sohl-Dickstein, J., Kingma, D. P., Kumar, A., Ermon, S., and Poole, B. Score-based generative modeling through stochastic differential equations. In *International Conference on Learning Representations*, 2021. URL <https://openreview.net/forum?id=PxtTIG12RRHS>.
- Wang, P.-W., Donti, P., Wilder, B., and Kolter, Z. Satnet: Bridging deep learning and logical reasoning using a differentiable satisfiability solver. In *International Conference on Machine Learning*, pp. 6545–6554. PMLR, 2019.
- Wei, J., Wang, X., Schuurmans, D., Bosma, M., Xia, F., Chi, E., Le, Q. V., Zhou, D., et al. Chain-of-thought prompting elicits reasoning in large language models. *Advances in neural information processing systems*, 35:24824–24837, 2022.
- Wu, Y., Sun, Z., Li, S., Welleck, S., and Yang, Y. An empirical analysis of compute-optimal inference for problem-solving with language models. 2024a.
- Wu, Y., Sun, Z., Li, S., Welleck, S., and Yang, Y. Inference scaling laws: An empirical analysis of compute-optimal inference for problem-solving with language models. *arXiv preprint arXiv:2408.00724*, 2024b.
- Yao, S., Yu, D., Zhao, J., Shafran, I., Griffiths, T., Cao, Y., and Narasimhan, K. Tree of thoughts: Deliberate problem solving with large language models. *Advances in Neural Information Processing Systems*, 36, 2024.

## A. Related algorithms and metric calculation

### A.1. Performance-energy Consistency

In this paper, performance-energy consistency refers to the consistency between the results evaluated using an energy model and those evaluated using real-world metrics for the same sample. Specifically, the consistency requires that good samples are assigned low energy, while poor samples are assigned high energy. Performance-energy consistency measures the proportion of element pairs that maintain the same relative order in both permutations  $X$  and  $Y$ , where  $X$  and  $Y$  represent the index arrays obtained by sorting the original energy values  $\mathbf{E} = (E_1, E_2, \dots, E_N)$  and performance metric values  $\mathbf{P} = (P_1, P_2, \dots, P_N)$ , respectively, in ascending order. In this paper, the energy values are calculated by energy model  $E_\theta(x_0)$  for samples  $x_0$ . The performance metric values are calculated as the L2 distance between the generated samples  $x_0$  and the ground truth under the given condition.

Let  $X = (X_1, X_2, \dots, X_N)$  and  $Y = (Y_1, Y_2, \dots, Y_N)$  be the index arrays obtained by sorting the original energy values  $\mathbf{E} = (E_1, E_2, \dots, E_N)$  and performance metric values  $\mathbf{P} = (P_1, P_2, \dots, P_N)$ , respectively, in ascending order. Specifically,  $X_i$  is the rank of the  $i$ -th sample in the sorted energy values  $\mathbf{E}$ , and  $Y_i$  is the rank of the  $i$ -th sample in the sorted performance metric values  $\mathbf{P}$ .

**Consistency Definition:** The **consistency** is defined as the proportion of consistent pairs  $(i, j)$  where  $i < j$  and the relative order of  $i$  and  $j$  in  $X$  is the same as in  $Y$ . Specifically:

$$\text{Consistency} = \frac{1}{\binom{N}{2}} \sum_{i=1}^{N-1} \sum_{j=i+1}^N \mathbb{I}((X_i < X_j \wedge Y_i < Y_j) \vee (X_i > X_j \wedge Y_i > Y_j)),$$

where:

- $\binom{N}{2} = \frac{N(N-1)}{2}$  is the total number of pairs  $(i, j)$  with  $i < j$ ,
- $\mathbb{I}[\cdot]$  is the indicator function, which evaluates to 1 if the condition inside the brackets holds (i.e., the relative order is consistent), and 0 otherwise.

### A.2. Adversarial sampling

During the sampling process, energy optimization often gets trapped in local minima or incorrect global minima, making it difficult to escape and hindering the sampling of high-quality samples.

### A.3. Negative Sample Generation

Negative samples are generated by introducing noise into the positive sample  $x_0$ . In the Maze and Sudoku experiments, permutation noise is applied to the channel dimension to induce significant changes in the solution. Other noise types can be used, as this remains a hyperparameter choice. Specifically, we first randomly sample two scalars  $p_1$  and  $p_2$  from a uniform distribution in the interval  $[0, 1]$ , i.e.,  $p_1, p_2 \sim \text{Uniform}(0, 1)$  ( $p_1 < p_2$ ). Then, for each channel position of the positive sample  $x_0$ , we swap the channel positions with probabilities  $p_1$  and  $p_2$ , resulting in  $x_0^-$  and  $x_0^{--}$ , such that the L2 distance between  $x_0^-$  and  $x_0$  is smaller than the L2 distance between  $x_0^{--}$  and  $x_0$ . For other noise types, such as Gaussian noise, we normalize the L2 norm of the noise and apply noise at different scales to ensure that the L2 distance from  $x_0^-$  to  $x_0$  is smaller than the L2 distance from  $x_0^{--}$  to  $x_0$ .

### A.4. Linear-regression algorithm

Given three points  $(x_1, y_1)$ ,  $(x_2, y_2)$ , and  $(x_3, y_3)$ , we wish to fit a line of the form (Lane et al., 2003):

$$y = kx + b$$

The mean of the  $x$ -coordinates and the mean of the  $y$ -coordinates are:

$$\bar{x} = \frac{1}{3}(x_1 + x_2 + x_3), \quad \bar{y} = \frac{1}{3}(y_1 + y_2 + y_3)$$

The slope  $k$  of the best-fit line is given by the formula:

$$k = \frac{\sum_{i=1}^3 (x_i - \bar{x})(y_i - \bar{y})}{\sum_{i=1}^3 (x_i - \bar{x})^2}$$

This formula represents the least-squares solution for the slope. Once the slope  $k$  is determined, the intercept  $b$  can be calculated as:

$$b = \bar{y} - k\bar{x}$$

The equation of the best-fit line is:

$$\hat{y} = kx + b$$

## B. Details of experiments

### B.1. Details of Sudoku experiments

For Sudoku experiment, the dataset, model architecture, and training configurations are adopted from Du et al. (2024). We mainly use solving success rate to evaluate different models. Model backbone and training configurations can be found in Fig. 4 and Table 5, respectively. All the exploration hyperparameters  $c$  are set as 100 for Sudoku task.

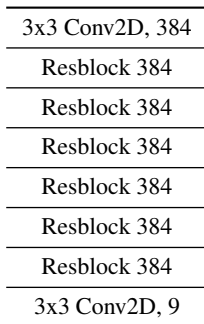


Figure 4. The model architecture for T-SCEND on Sudoku task. The energy value is computed using the L2 norm of the final predicted output similar to Du et al. (2023), while the output is directly used as noise prediction for the diffusion baseline.

Table 5. Details of training for Sudoku task.

Training configurations	
Number of training steps	100000
Training batch size	64
Learning rate	0.0001
Diffusion steps	10
Inner loop optimization steps	20
Denoising loss type	MSE
Optimizer	Adam

### B.2. Details of Maze experiments

The details of maze experiments and model backbone are provided in Table 6 and Fig. 5, respectively. The key metric, the maze-solving success rate is defined as the proportion of model-generated paths that have no breakpoints, do not overlap with walls, and begin and end at the start and target points, respectively. Maze datasets are generated by Ivanitskiy et al. (2023), and detailed hyperparameter configurations are in Table 6. All the exploration hyperparameters  $c$  are set as 100 for Maze task.

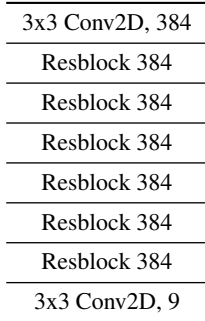


Figure 5. The model architecture for T-SCEND on Maze task. The energy value is computed using the L2 norm of the final predicted output similar to Du et al. (2023), while the output is directly used as noise prediction for the diffusion baseline.

Table 6. Details of Maze dataset, training.

Dataset:	
Size of training dataset with grid size 4	10219
Size of training dataset with grid size 5	9394
Size of training dataset with grid size 6	10295
Minimum length of solution path	5
Algorithm to generate the maze	DFS
Size of test dataset with grid size 6	837
Size of test dataset with grid size 8	888
Size of test dataset with grid size 10	948
Size of test dataset with grid size 12	960
Size of test dataset with grid size 15	975
Size of test dataset with grid size 20	978
Size of test dataset with grid size 30	994
Training configurations	
Number of training steps	200000
Training batch size	64
Learning rate	0.0001
Diffusion steps	10
Inner loop optimization steps	20
Denosing loss type	MSE + MAE
Optimizer	Adam

### C. Performance sensitivity to hyperparameters

In this subsection, we analyze the impact of several hyperparameters on the experimental results. As shown in Table 8, the influence of different noise scales on the performance of various methods is presented. The hMCTS denoising and random search require a relatively larger noise scale to better expand the search space and improve final performance, while the diffusion model with naive inference performs best with a smaller noise scale. As demonstrated in Table 7 and Fig. 6, the effect of varying inner-loop optimization steps on the results is also analyzed. It can be observed that performance improves gradually with an increasing number of steps, and after 5 steps, the performance stabilizes and the improvement slows down. Therefore, we chose 5 inner-loop optimization steps for the Maze experiments in this paper.

### D. Additional results

The parameter  $t_s$  controls the proportion of the total inference budget allocated to MCTS denoising. When  $t_s = 9$ , it means only MCTS denoising is used, while  $t_s = 0$  means only best-of-N random search is employed. For  $0 < t_s < 9$ , hMCTS denoising is applied. As shown in Table 9 and Fig. 7, there is a noticeable peak in model performance as  $t_s$  varies.

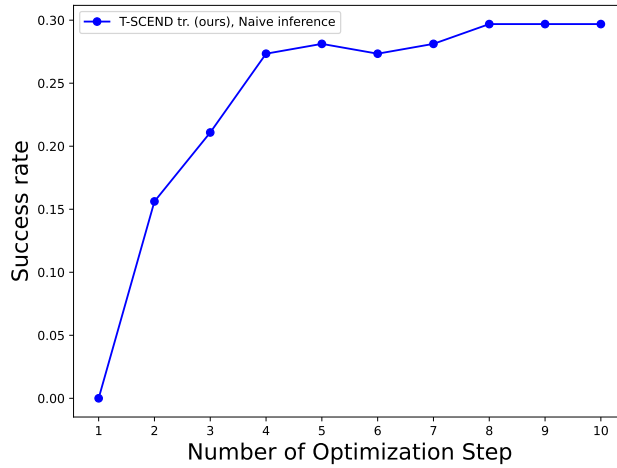


Figure 6. Visualization of success rate across different number of inner-loop optimization steps on Maze with grid size  $15 \times 15$ .

Table 7. Success rate across the different number of inner-loop optimization step on Maze with grid size  $15$ .

Methods	Number of optimization step									
	1	2	3	4	5	6	7	8	9	10
T-SCEND tr. (ours), Naive inference	0.0000	0.1562	0.2109	0.2734	0.2812	0.2734	0.2812	0.2969	0.2969	0.2969

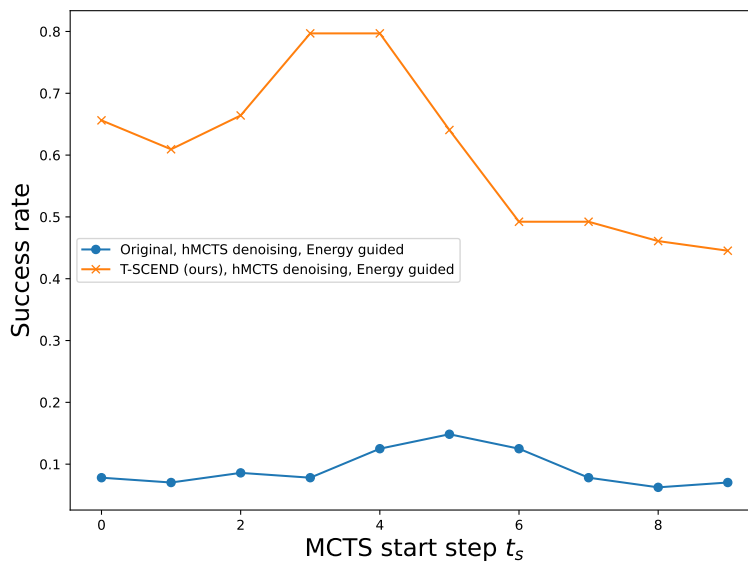


Figure 7. Visualization of Success rate across different MCTS start step  $t_s$ .

### E. Limitations and future work

Our inference framework primarily relies on MCTS, which presents two key limitations: (1) limited compatibility with parallel computing, and (2) challenges in effectively evaluating node quality during the early stages of denoising. Future

Table 8. Success rate across different noise scales on Maze with grid size 15.

Methods	Noise scale									
	0.1	0.2	0.3	0.4	0.5	0.6	0.7	0.8	0.9	1.0
T-SCEND tr. (ours), hMCTS denoising (energy)	0.3828	0.4375	0.5312	0.6094	0.6562	0.6953	0.7031	0.7344	0.7734	0.7969
T-SCEND tr. (ours), naive inference	0.3125	0.2656	0.2578	0.2344	0.2422	0.2656	0.2578	0.2422	0.2500	0.2500
T-SCEND tr. (ours), Random search(energy)	0.3906	0.4453	0.5312	0.5703	0.5938	0.6328	0.6641	0.6719	0.6797	0.6562

Table 9. Success rate of hMCTS denoising on Maze with grid size 15 across different MCTS start steps.

Methods	0	1	2	3	4	5	6	7	8	9
Original, hMCTS denoising (energy)	0.0781	0.0703	0.0859	0.0781	0.1250	0.1484	0.1250	0.0781	0.0625	0.0703
T-SCEND tr. (ours), hMCTS denoising (energy)	0.6562	0.6094	0.6641	0.7969	0.7969	0.6406	0.4922	0.4922	0.4609	0.4453

Table 10. Success rate of Random search for different training methods on Maze with grid size 15 and Sudoku harder dataset guided with ground truth accuracy. Untrained, Random search (gt) represents use ground truth to guide the random search. Here,  $L = N$ . Bold font denotes the best model.

Methods	Maze success rate						Sudoku success rate						
	$N=1$	$N=11$	$N=21$	$N=41$	$N=81$	$N=161$	$N=1$	$N=11$	$N=21$	$N=41$	$N=81$	$N=161$	$N=321$
Untrained, Random search (gt)	0.0000	0.0000	0.0000	0.0000	0.0000	0.0000	0.0000	0.0000	0.0000	0.0000	0.0000	0.0000	0.0000
Original, Random search (gt)	0.0625	0.1250	0.1094	0.1328	0.1719	0.1719	0.0859	0.1641	0.2188	0.2344	0.2422	0.2656	0.2969
DDPM, Random search (gt)	0.0312	0.1094	0.1587	0.1746	0.2031	0.2422	0.0000	0.0000	0.0000	0.0000	0.0000	0.0000	0.0156
T-SCEND tr. w/o LRNCL, Random search (gt)	<b>0.2500</b>	<b>0.5078</b>	<b>0.5938</b>	<b>0.6562</b>	<b>0.7109</b>	<b>0.7422</b>	<b>0.1094</b>	<b>0.2578</b>	<b>0.2969</b>	<b>0.3438</b>	<b>0.3750</b>	<b>0.3828</b>	<b>0.4219</b>

Table 11. Success rate and element-wise accuracy of Random search for different training methods on Sudoku harder dataset guided with ground truth accuracy. Here,  $L = N$ . Bold font denotes the best model.

Methods	Success rate							Element-wise accuracy						
	$N=1$	$N=11$	$N=21$	$N=41$	$N=81$	$N=161$	$N=321$	$N=1$	$N=11$	$N=21$	$N=41$	$N=81$	$N=161$	$N=321$
DDPM, Random search, GT accuracy guided	0.0000	0.0000	0.0000	0.0000	0.0000	0.0000	0.0156	0.5071	0.6089	0.6316	0.6492	0.6691	0.6881	0.6999
Original, Random search, GT accuracy guided	0.0781	0.1641	0.2188	0.2344	0.2422	0.2656	0.2812	<b>0.6650</b>	0.7731	0.7952	0.8036	0.8217	0.8347	0.8491
T-SCEND tr. w/o LRNCL, Random search, GT accuracy guided	<b>0.1094</b>	<b>0.2578</b>	<b>0.2969</b>	<b>0.3438</b>	<b>0.3750</b>	<b>0.3828</b>	<b>0.4219</b>	0.6442	<b>0.7855</b>	<b>0.8096</b>	<b>0.8317</b>	<b>0.8466</b>	<b>0.8628</b>	<b>0.8854</b>

work could explore integrating alternative search strategies, such as those proposed by Wu et al. (2024b). Additionally, to enhance performance-energy consistency, we introduce linear-regression negative contrastive learning, which enforces a linear relationship between energy and the distance to real samples. Further investigation is needed to assess the broader implications of this constraint and explore alternative regularization approaches. Lastly, while our current implementation utilizes Gaussian noise for branching, other diffusion-based branching mechanisms remain an open area for exploration.

## F. Visualization of results

### F.1. Visualization of Maze experiments

This section presents visualizations of the training in Fig. 8, test Maze data in Fig. 9, and samples generated by different methods in Fig. 10. In the visuals, black pixels denote walls, green represents the starting point, red represents the goal point, blue marks the solved path, and white represents the feasible area. All visualizations are based on a few representative samples. The results from the training and test sets clearly show that the tasks in the test set are notably more challenging than those in the training set. Visual comparisons of samples generated by different methods reveal that the originally trained model, regardless of the inference strategy, performs consistently worse than T-SCEND.

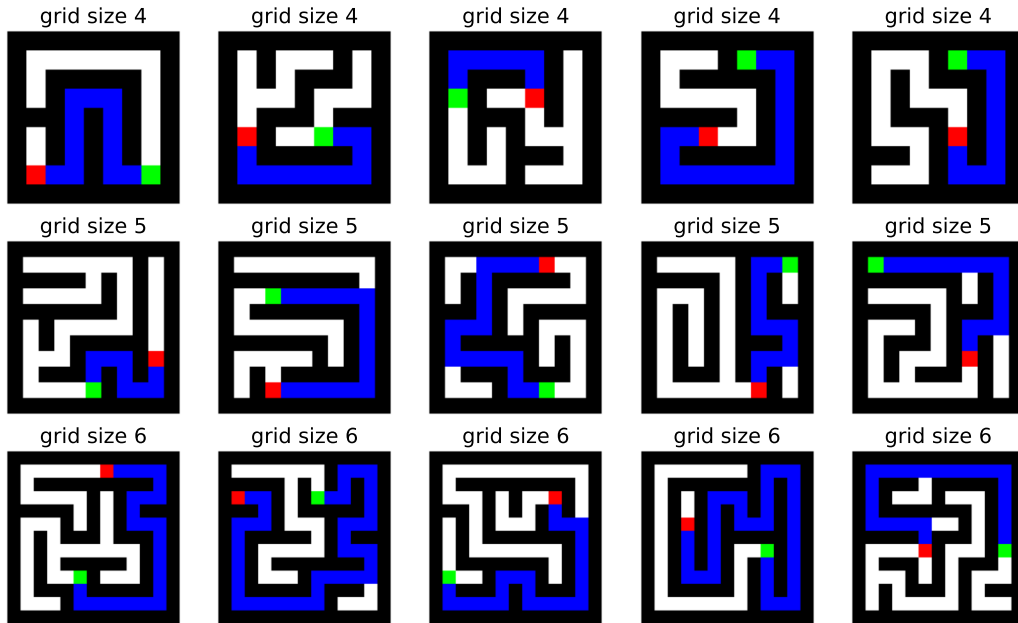


Figure 8. Visualization of training maze dataset.

## F.2. Visualization of Sudoku experiments

This section presents visualizations of the training and test Sudoku data in Fig. 11, and representative samples generated by different methods in Fig. 12. In the visuals, black numbers denote the condition, green numbers represent correct predictions, and red numbers represent wrong predictions. All visualizations are derived from a few representative samples. The comparison between the training and test sets clearly indicates that the tasks in the test set are significantly more difficult than those in the training set. When comparing the samples generated by different methods, it is evident that the originally trained model, regardless of the inference strategy, consistently underperforms compared to T-SCEND.



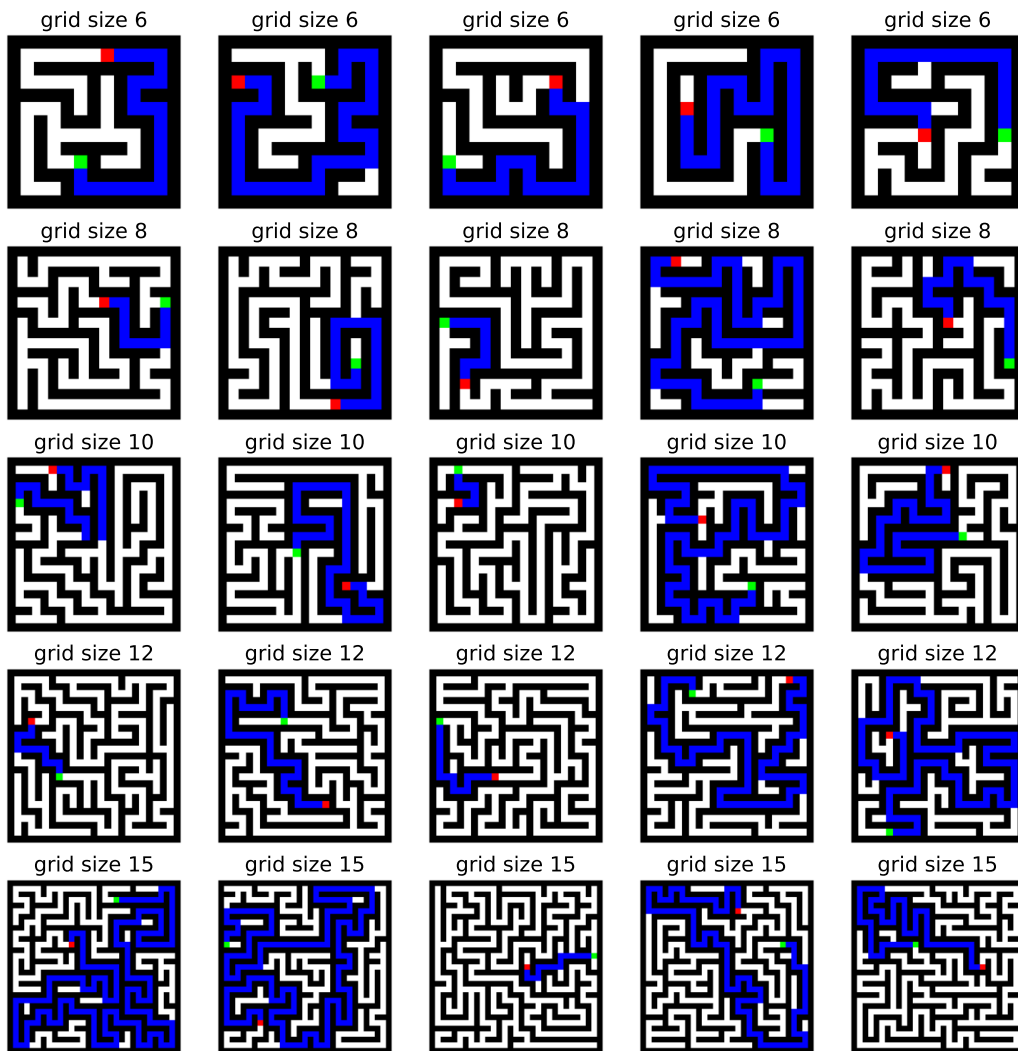


Figure 9. Visualization of test maze dataset, where the blue paths are ground-truth solutions.

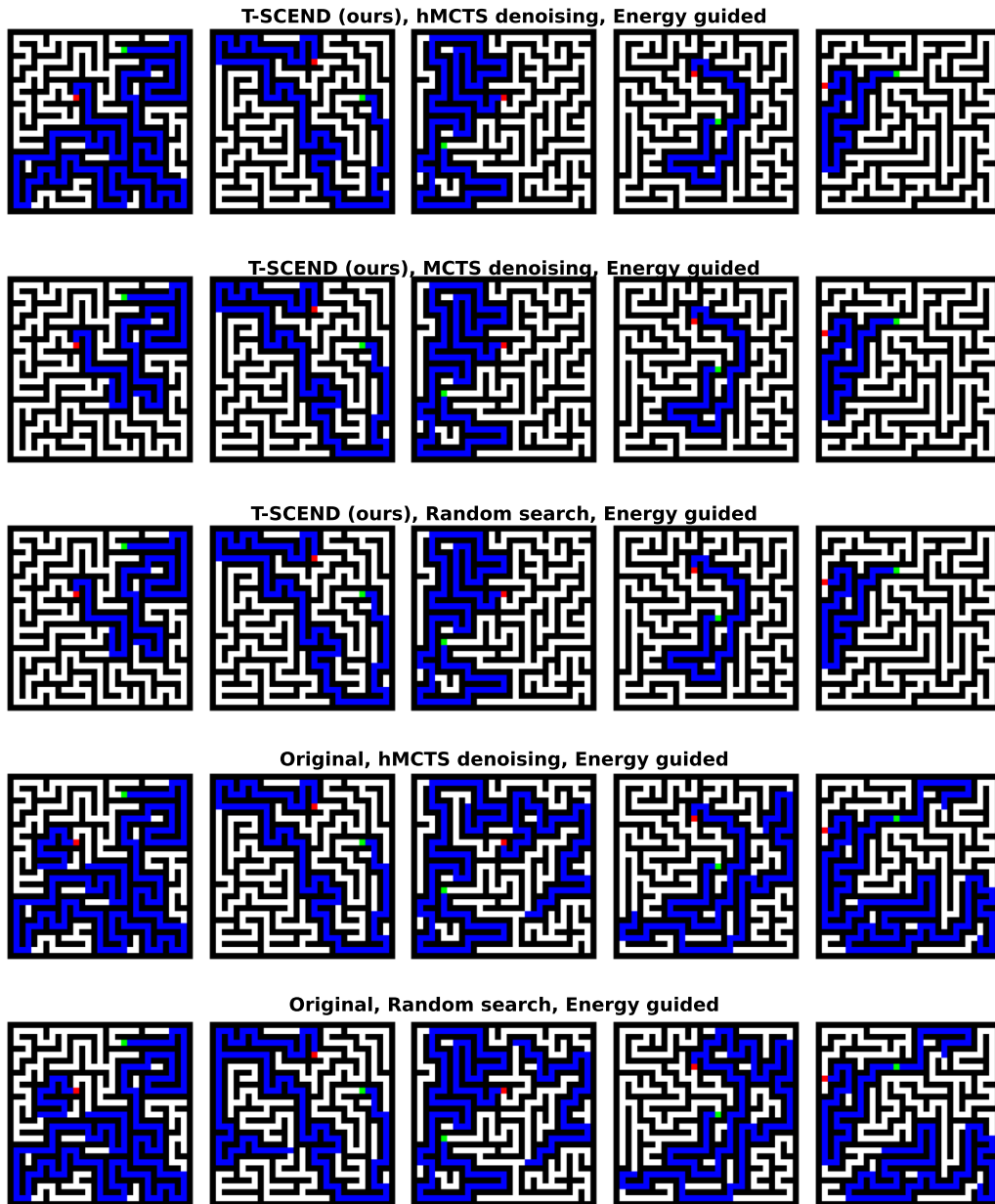


Figure 10. Visualization of samples generated by different training and inference methods.

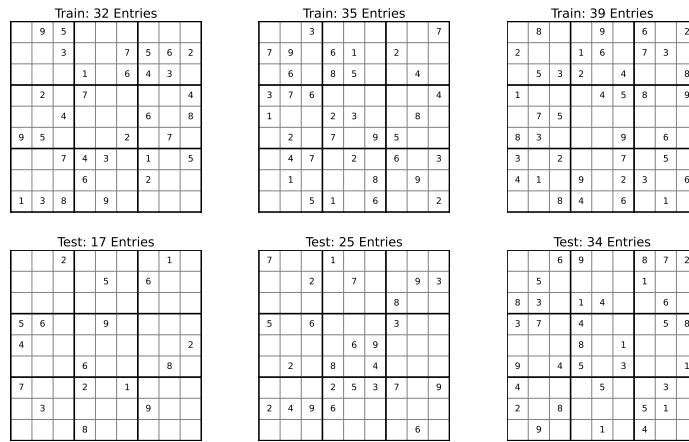


Figure 11. Visualization of training and test Sudoku dataset.

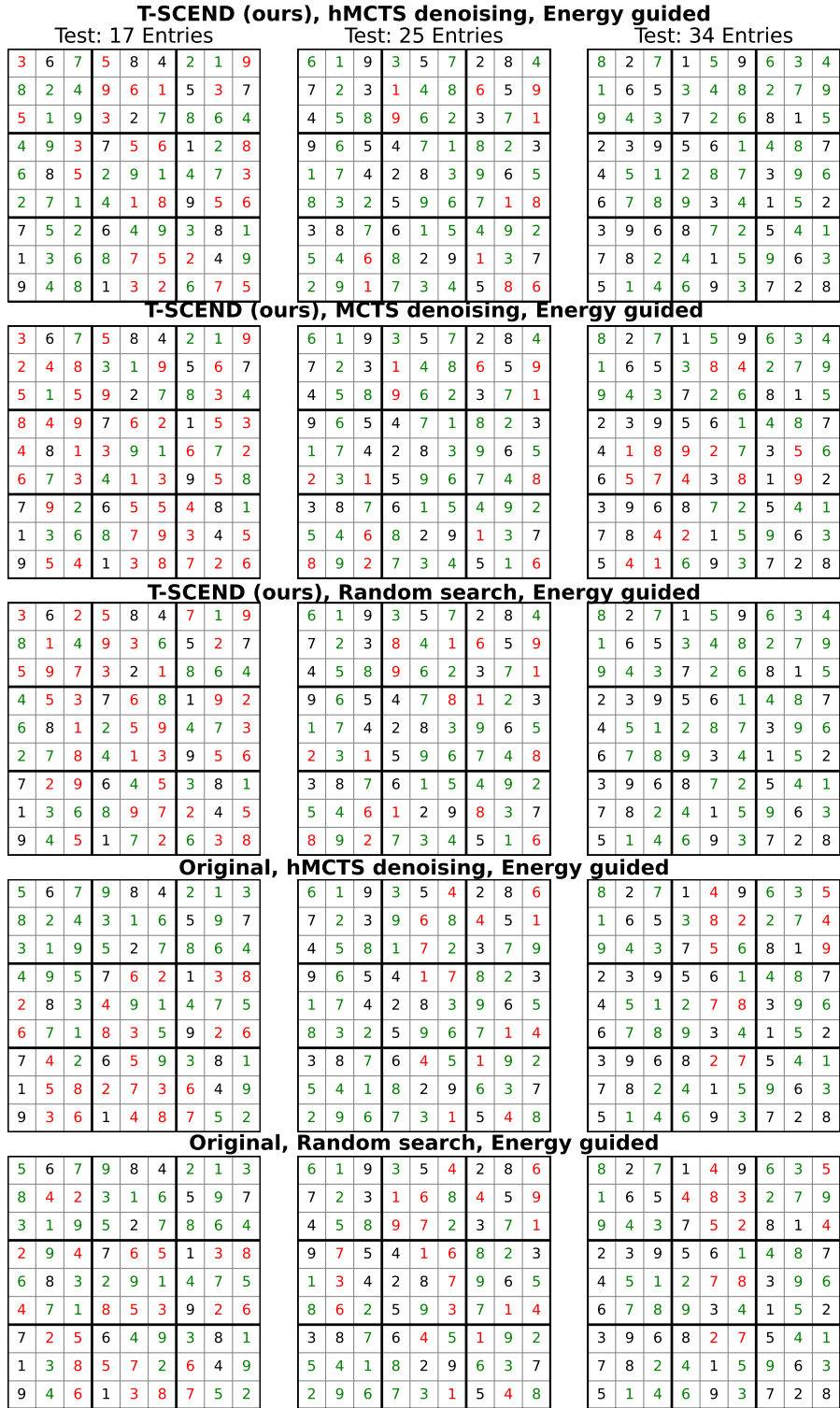


Figure 12. Visualization of samples generated by different training and inference methods.